Spectral Hong-Ou-Mandel Effect between a Heralded Single-Photon State and a Thermal Field: Multiphoton Contamination and the Nonclassicality Threshold

Anahita Khodadad Kashi,[1,2] Lucia Caspani,[3] and Michael Kues[1,2]
[1]Institute of Photonics, Leibniz University Hannover, 30167 Hannover, Germany
[2]Cluster of Excellence PhoenixD (Photonics, Optics, Engineering—Innovation Across Disciplines), Leibniz University Hannover, 30167 Hannover, Germany
[3]Institute of Photonics, Department of Physics, University of Strathclyde, Glasgow G1 1RD, United Kingdom

(Received 20 February 2023; accepted 16 October 2023; published 4 December 2023)

The Hong-Ou-Mandel (HOM) effect is crucial for quantum information processing, and its visibility determines the system's quantum-classical characteristics. In an experimental and theoretical study of the spectral HOM effect between a thermal field and a heralded single-photon state, we demonstrate that the HOM visibility varies dependent on the relative photon statistics of the interacting fields. Our findings reveal that multiphoton components in a heralded state get engaged in quantum interference with a thermal field, resulting in improved visibilities at certain mean photon numbers. We derive a theoretical relationship for the HOM visibility as a function of the mean photon number of the thermal field and the thermal part of the heralded state. We show that the nonclassicality degree of a heralded state is reflected in its HOM visibility with a thermal field; our results establish a lower bound of 41.42% for the peak visibility, indicating the minimum assignable degree of nonclassicality to the heralded state. This research enhances our understanding of the HOM effect and its application to high-speed remote secret key sharing, addressing security concerns due to multiphoton contamination in heralded states.

DOI: 10.1103/PhysRevLett.131.233601

Introduction.—Large-scale quantum networks enable secure remote transfer of quantum states. Such capability relies on highly efficient, noise-resistant, and robust quantum internet components [1], ranging from quantum end nodes to interconnects and repeaters [2,3]. At the heart of a quantum network lies the Hong-Ou-Mandel (HOM) effect [4–7] which involves destructive quantum interference at a balanced beam splitter of both-reflected and both-transmitted two-photon amplitudes. Frequency encoding is a promising platform for global quantum networks, thanks to its parallelizability, phase stability, noise resilience, and compatibility with modern telecommunications infrastructure [8,9]. Moreover, frequency allows for reversible conversion of quantum states among various physical systems within a quantum network [10,11]. Recent advancements include a scalable realization of the spectral HOM effect between independent single-photon states [12]. The HOM effect underpins the development of measurement-device-independent quantum key distribution (MDI-QKD) protocols, addressing the side-channel security gaps [13–16] and, in particular, implemented between imperfect single-photon sources—such as heralded states from spontaneous parametric down-conversion (SPDC) [17]—and weak classical states [16,18–21]. To enable quantum interference, preparing single-mode heralded single-photon states involves eliminating frequency correlations. This introduces thermal characteristics to the state, the impact of which has not been explicitly studied on the HOM visibility.

Here, we experimentally implement the spectral HOM effect between a thermal field and a heralded single-photon state from pulsed-excited SPDC process. We analyze the impact of multiphoton contamination in imperfect single-photon states on the HOM visibility. Importantly, our findings reveal that multiphoton components in a heralded state contribute to quantum interference with the thermal field. This observation questions the common assumption that multiphoton components in a heralded state exclusively degrade the visibility, hence subtracted from the coincidence counts (CC) [22]. This study provides fundamental insight into the link between the HOM visibility and photon statistics of the interacting fields, with potential application in ascertaining security in high-speed remote secret key sharing [23].

Theoretical derivation of visibility in the HOM interference between a thermal field and a heralded state.—In a pulsed-driven SPDC process with a two-mode squeezer (Fig. 1), a single detection in the signal mode s1 (on detector D3) heralds the existence of at least one photon in the idler mode i1 (on detector D1), resulting in a heralded state in the latter mode. The first- and the second-order moments associated with the heralded state are

$$\langle \hat{a}^{\dagger}\hat{a}\rangle_{i1} = \mathrm{Tr}\{\hat{a}_{i1}^{\dagger}\hat{a}_{i1}\tilde{\rho}^{i}\} = \bar{n}_{\mathrm{i1,th}} + 1$$
$$\langle \hat{a}^{\dagger 2}\hat{a}^{2}\rangle_{i1} = \mathrm{Tr}\{\hat{a}_{i1}^{\dagger 2}\hat{a}_{i1}^{2}\tilde{\rho}^{i}\} = 2\bar{n}_{\mathrm{i1,th}}^{2} + 2\bar{n}_{\mathrm{i1,th}}, \quad (1)$$

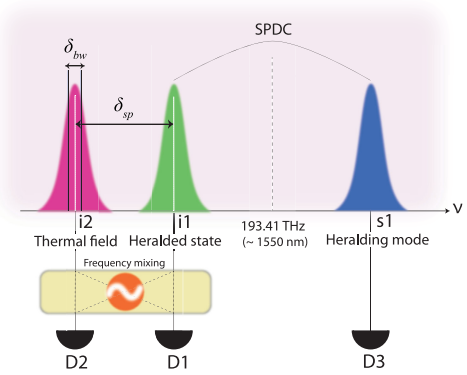

FIG. 1. Spectral configuration of the spectral HOM experiment between a thermal field (i2: red) and a heralded single-photon state (i1: green); electro-optic phase modulation (frequency mixing) is applied between i1 and i2. (insertion loss: 2.8 dB, $\delta_{\mathrm{sp}} = 75$ GHz; $\delta_{\mathrm{bw}} = 22$ GHz; rf tone $\Omega = 25$ GHz; rf power amplitude: -10 dB; ν: frequency axis).

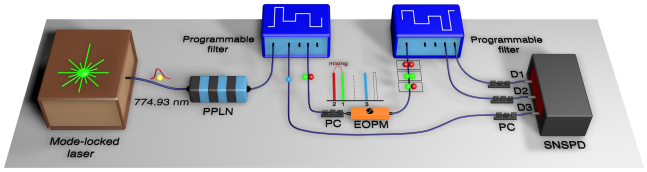

FIG. 2. Experimental setup of the spectral HOM effect between a thermal field and a heralded state. A single excitation photon (yellow) is sent through a PPLN waveguide and decays into pairs of correlated signal-idler photons. The system's spectral configuration is defined at the first programmable filter. The idler photon i1 (green) is heralded by the detection of its twin photon in the signal mode s1 (blue), and the idler mode i2 (red) is detected independently but triggered by detections on s1. Electro-optic phase modulation is applied on the idler modes i1 and i2, and the coincidence detections are collected on detectors D1 (monitoring i1), D2 (monitoring i2), and D3 (monitoring s1). [polarization controller (PC); electro-optic phase modulator (EOPM); superconducting nanowire single photon detector (SNSPD)].

where $\tilde{\rho}^i$ is the normalized density matrix describing the heralded state (see Sec. I in the Supplemental Material [24], and Ref. [25]). The $\hat{a}_{i1}^{\dagger}$ and $\hat{a}_{i1}$ are the photon creation and annihilation operators, respectively, and $\bar{n}_{i1,\mathrm{th}}$ represents the average photon number per pulse period within the thermal part of the heralded state, i.e., the multiphoton components. The thermal field is created in the idler frequency mode i2 from an independent SPDC process and by discarding the detections on its twin signal frequency mode (see Fig. 1). From Eq. (1), the second-order correlation between the thermal field and the heralded state is derived as a function of the photons' arrival times t and t' at the detectors (see Sec. II [24] and Ref. [26])

$$g^{(2)}_{i1,i2}(t,t') = 2\bar{n}^2_{i1,\mathrm{th}} + 2\bar{n}^2_{i2} + 2\bar{n}_{i1,\mathrm{th}} + 2\bar{n}_{i2}(\bar{n}_{i1,\mathrm{th}} + 1)(1 - \delta_{i1,i2}) \quad (2)$$

with $\bar{n}_{i2}$ as the mean photon number per pulse period of the thermal field triggered by detections on s1. The modulation coefficient $\delta_{\mathrm{i1,i2}} \in [0, 1]$ depends on the fields' degree of indistinguishability. From (2) we derived a new relationship between the HOM visibility and $\bar{n}_{i1,\mathrm{th}}$ and $\bar{n}_{i2}$ (see Sec. II [24]):

$$V_{\mathrm{theory}} = \frac{1}{1 + \dfrac{\bar{n}^2_{i1,\mathrm{th}} + \bar{n}^2_{i2} + \bar{n}_{i1,\mathrm{th}}}{\bar{n}_{i1,\mathrm{th}}\bar{n}_{i2} + \bar{n}_{i2}}}. \quad (3)$$

Experimental implementation of the HOM effect between a thermal field and a heralded state.—The experimental setup (see Fig. 2) includes a mode-locked laser (*Menlo Systems*) with 50 MHz repetition rate, centered at $\lambda_{\mathrm{pump}} =$ 774.93 nm wavelength, and filtered to full width at half maximum $\mathrm{FWHM}_{\mathrm{pump}} = 200$ GHz. A 40 mm-long, 5% MgO-doped PPLN waveguide (*Covesion*) is used to create time-energy correlated signal-idler photon pairs via SPDC, centered around the degeneracy point $\lambda_{\mathrm{deg}} \sim 1550$ nm. The spectral configuration (See Fig. 1) was adjusted using a programmable filter (*Finisar Waveshaper 4000S*; insertion loss: 4.5 dB) to guarantee high spectral purity of the photons (single-mode bandwidth $\delta_{\mathrm{SMB}} \sim 50$ GHz; see HBT interferometry in Sec. III [24] and Refs. [12,27–30]). Electro-optic phase modulation (EOPM; *EO Space*) is used to half split the power between the heralded state (i1) and the thermal field (i2) enabling to probe the HOM effect in frequency (see Refs. [12,31] and Sec. IV in [24]). The sidebands are generated at 25 GHz free spectral range and band-pass filtered to maintain the experiment's spectral configuration. Coincidence events are recorded at integer multiples of the 20 ns pulse period via a timing electronics module (*Swabian instruments; Timetagger Ultra*).

Experimental retrieval of visibility for the HOM effect between a thermal field and a heralded state.—The experimental result of the spectral HOM effect is shown in Fig. 3. The threefold coincidence counts are displayed versus delay—expressed as integer multiples of the pulse period ($\Delta t = m \times T$; $T = 20$ ns; $m = 0, \pm 1, \pm 2, \ldots$)—between D2 and the heralded detections on D1. In general, visibility in the HOM effect is probed by contrasting the number of two-photon amplitudes of indistinguishable photons (from two input modes of a beam splitter) that bunch in the output modes, to those of distinguishable photons that emerge as coincidence detections, the latter considered as reference point $\mathrm{CC}_{\mathrm{ref}}$. Distinguishability is achievable by introducing nonzero delay values Δt between the photons. In conventional HOM setups [22,32], temporal distinguishability is realized between the two input modes of a beam splitter via an optical delay line. Unlike such approaches where the average delayed coincidence counts serve as the reference point $\mathrm{CC}_{\mathrm{ref}} = \mathrm{CC}^{\mathrm{ave}}(\Delta t \neq 0)$, the

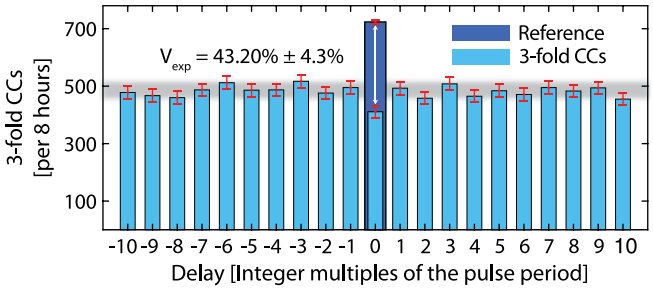

FIG. 3. Results from the spectral HOM experiment between a thermal field and a heralded state: Threefold coincidence counts as a function of delay between detectors D1 and D2—triggered by single detections on D3. The gray line shows the average number of delayed coincidence counts $CC^{\mathrm{ave}}(\Delta t \neq 0) = 484 \pm 22$. The arrow shows the experimental value for HOM visibility, $V_{\mathrm{exp}} = 43.2\% \pm 4.3\%$, defined as the difference between the reference point, $CC_{\mathrm{ref}} = 724 \pm 45$, and the coincidence counts measured at zero delay, $CC(0) = 411 \pm 20$. The error bars show the standard deviation (square root) of the coincidence counts per 8-hour integration time.

interpulse delay principle ($\Delta t = m \times T$; $T = 20$ ns; $m = 0, \pm 1, \pm 2, \ldots$) adopted in our experiment necessitates considering additional coincidence counts to determine $\mathrm{CC}_{\mathrm{ref}}$ (see Sec. V in the Supplemental Material [24]). Such enhancement in CCs is associated with the thermal statistics of multiphoton components in the heralded state. We can distinguish three contributions: The threefold CCs from photons residing prior to phase modulation in different input modes $\mathrm{CC}_{\mathrm{i2,i1|s1}}$, from multiphoton components within the thermal field $\mathrm{CC}_{\mathrm{i2,i2|s1}}$, and from multiphoton components within the heralded state $\mathrm{CC}_{\mathrm{i1,i1|s1}}$. The reference point is thus written

$$\mathrm{CC}_{\mathrm{ref}} = A \times \mathrm{CC}_{\mathrm{i1,i1|s1}}(\Delta t \neq 0) + B \times \mathrm{CC}_{\mathrm{i2,i2|s1}}(\Delta t \neq 0) + \mathrm{C} \times \mathrm{CC}_{\mathrm{i2,i1|s1}}(\Delta t \neq 0). \quad (4)$$

The HOM visibility V_{exp} is obtained through

$$V_{\mathrm{exp}} = [\mathrm{CC}_{\mathrm{ref}} - \mathrm{CC}(0)]/\mathrm{CC}_{\mathrm{ref}} \quad (5)$$

with CC(0) as the threefold coincidence counts measured at zero delay ($\Delta t = 0$). On the right-hand side of Eq. (4), D1 and D2 detect photons exclusively emitted from i1 (first term), exclusively from i2 (second term), and from both i1 and i2 (third term). The enhancement coefficients $A = g^{(2)}_{\mathrm{i1,i1|s1}}(0)$ and $B = g^{(2)}_{\mathrm{i2,i2|s1}}(0)$, which account for the additional CCs introduced by multiphoton components, are defined as the unconditional second-order auto-correlation functions

$$g^{(2)}_{\mathrm{i1(i2),i1(i2)|s1}}(0) = \mathrm{CC}_{\mathrm{i1(i2),i1(i2)|s1}}(0)/\mathrm{CC}_{\mathrm{i1(i2),i1(i2)|s1}}(\Delta t \neq 0). \quad (6)$$

The enhanced CCs result from high spectral purity and temporal indistinguishability at zero delay, essential for implementing the HOM effect [27,33,34]. By exclusively allowing the emission from i1 (i2) and s1 to pass through the first programmable filter, the unconditional second-order auto-correlation function $A = 1.98 \pm 0.1$ ($B \approx 2$) for the heralded-state in i1 (thermal field in i2) is measured (see Sec. VI [24]), which confirms the single frequency-mode assumption. However, the contribution from the second term is found negligible for the delayed and nondelayed events $\mathrm{CC}_{\mathrm{i2,i2|s1}}(\Delta t \neq 0) \approx \mathrm{CC}_{\mathrm{i2,i2|s1}}(\Delta t = 0) \approx 0$ which ascribes to three SPDC processes per pulse. For the last term we obtain C = 1, namely, the threefold coincidence detections from two different input modes i1 and i2, emerge at an identical delayed and nondelayed rate, $\mathrm{CC}_{\mathrm{i2,i1|s1}}(\Delta t \neq 0) = \mathrm{CC}_{\mathrm{i2,i1|s1}}(\Delta t = 0)$. This owes to the fact that generation in i1 and i2 emerge from two different SPDC processes. Since the separation bandwidth between i1 and i2 exceeds the single-mode bandwidth (50 GHz; see Sec. III [24]), i1 and i2 are considered independent spectral modes. As a result, the generation rate of photons in i1 and i2, whether in different pulses or the same pulse, is identical. In this experiment, the average delayed threefold coincidence counts are measured $\mathrm{CC}^{\mathrm{ave}}(\Delta t \neq 0) = 484 \pm 22$, which consists in the following events: $\mathrm{CC}^{\mathrm{ave}}(\Delta t \neq 0) = \mathrm{CC}^{\mathrm{ave}}_{\mathrm{i1,i1|s1}}(\Delta t \neq 0) + \mathrm{CC}^{\mathrm{ave}}_{\mathrm{i2,i1|s1}}(\Delta t \neq 0)$; the contribution of each constituent term is obtained by having access to the generation ratio $\bar{n}_{i1,\mathrm{th}}/\bar{n}_{i2} \approx 1.02$ between the mean photon number per pulse period of the thermal part of the heralded state, $\bar{n}_{i1,\mathrm{th}}$, and the thermal field, $\bar{n}_{i2}$ (see Sec. VII [24]). From this ratio the first $\mathrm{CC}^{\mathrm{ave}}_{\mathrm{i1,i1|s1}}(\Delta t \neq 0) \approx 245$ and second terms $\mathrm{CC}^{\mathrm{ave}}_{\mathrm{i2,i1|s1}}(\Delta t \neq 0) \approx 239$ are retrieved. From Eq. (4), the reference point $\mathrm{CC}_{\mathrm{ref}} \approx 724 \pm 45$ is thus determined. From the measured coincidence counts at zero delay, $\mathrm{CC}(0) = 411 \pm 20$, the experimental HOM visibility, $V_{\mathrm{exp}} = 43.2\% \pm 4.3\%$, is calculated.

Validating the experimental results.—Assuming $P(n)$ as the probability of having n heralded photons per heralding detection, for a heralded state characterized by $P(1) \gg P(2) \gg P(n > 2)$, the following relations hold true [34]

$$g^{(2)}_h(0) \approx 2P(2)/P(1)^2$$
$$P(0) + P(1) + P(2) + P(n > 2) = 1, \quad (7)$$

where $g^{(2)}_h(0) \approx 0.25$ is the measured heralded autocorrelation function (see Sec. VIII [24]). In our system for $n > 2$ we assume $P(n > 2) \approx 0$. In addition, we have $P(0) \approx 0$, which denotes zero probability of occupation in the vacuum

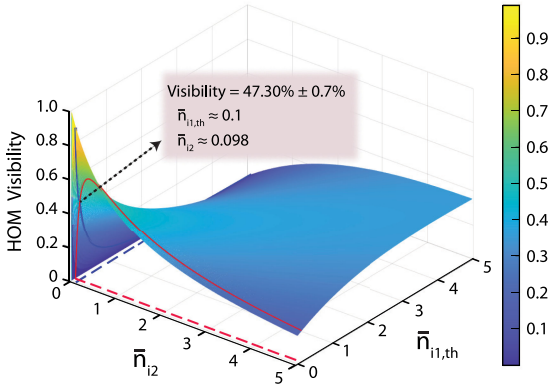

FIG. 4. Visibility of the HOM interference between a thermal field and a heralded state, as a function of the average photon number per pulse period of the thermal field ($\bar{n}_{i2}$) and the thermal part of the heralded state ($\bar{n}_{i1,th}$). The dashed arrow points to the intersection of the experimentally measured mean photon numbers $\bar{n}_{1,th} \approx 0.1$ and $\bar{n}_{i2} \approx 0.098$, in turn corresponding to the theoretical value of the HOM visibility $V_{theory} \approx 47.3 \pm 0.7\%$.

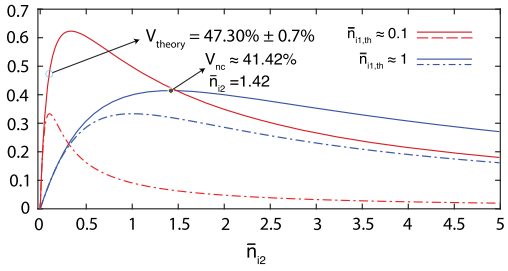

FIG. 5. HOM visibility versus $\bar{n}_{i2}$ for fixed values of $\bar{n}_{i1,th} = 0.1$ and $\bar{n}_{i1,th} = 1$, corresponding to the experimental value and the nonclassicality upper threshold of the multiphoton components in the heralded state. The $V_{theory} \approx 47.3\% \pm 0.7\%$ is our theoretical HOM visibility under $\bar{n}_{i1,th} \approx 0.1$ and $\bar{n}_{i2} \approx 0.098$.

state for a heralded state. From Eq. (7) the probabilities $P(1) \approx 0.89$ and $P(2) \approx 0.1$ are determined. Followed by $\bar{n}_{i1} = \mathrm{Tr}\{\hat{\rho}_{i1}\hat{n}_{i1}\}$ with $\hat{n}_{i1}$ as the mean photon number in the heralded state, $\hat{n}_{i1}$ as the photon number operator, and $\hat{\rho}_{i1} = \sum_n P(n)|n\rangle\langle n|$ as the density matrix of the heralded state, $\bar{n}_{i1} = P(1) + 2P(2)$ is yielded, hence $\bar{n}_{i1} \approx 1.1$. Subtraction of the single-photon contribution from $\bar{n}_{i1}$ gives $\bar{n}_{i1,th} \approx 0.1$. The generation ratio $\bar{n}_{i1,th}/\bar{n}_{i2} \approx 1.02$ thus gives $\bar{n}_{i2} \approx 0.098$. By replacing $\bar{n}_{i1,th}$ and $\bar{n}_{i2}$ in Eq. (3), the visibility $V_{theory} = 47.3\% \pm 0.7\%$ for the HOM effect between the heralded state and the thermal field is obtained, which is in good agreement with the experimental result from the previous section.

Discussion.—By definition the HOM effect is considered as a two-photon bunching effect that results from the superposition on a balanced beam splitter of two indistinguishable photons, coming from different input modes of the beam splitter. This definition establishes the presumption of full involvement in the HOM effect—under perfect indistinguishability—for the two-photon amplitudes from i1 and i2, hence leading to zero coincidence counts at zero delay ($CC_{i2,i1|s1}(0) = 0$). In contrast, the threefold events from multiphoton components in the heralded state i1 were presumed to remain intact as a result of emerging from two photons in the same frequency mode, i.e., perceived as background terms. On this account, a minimum predicted value $CC_{pr}(0) = CC_{i1,i1|s1}(0) \sim 485 \pm 40$ was foreseen for the nondelayed coincidence counts—considering the enhancement coefficient. However, in experiment $CC(0) = 411 \pm 20$ was measured, which falls outside the standard deviation range and below the minimum predicted amount $CC_{pr}(0)$. Importantly, as conducted in previous works [22] subtraction of $CC_{i1,i1|s1}(0)$ from CC(0)—if assumed as background—would lead to negative values, hence proved unphysical. The difference between experiment and initial expectation is explainable by engagement of heralded state multiphoton components in the HOM effect with the thermal field. This is verified by the theory derived in Eq. (3) and illustrated in Fig. 4 showing the dependency of the HOM visibility on $\bar{n}_{i2}$ and $\bar{n}_{i1,th}$. The dashed arrow shows the conjunction between $\bar{n}_{i2}$ and $\bar{n}_{i1,th}$ from experiment and the corresponding visibility. Under $n_{i2} \ll 1$ and for $\bar{n}_{i1,th} = 0$, 100% visibility is achievable. For increasing values of $\bar{n}_{i1,th}$, the visibility decreases as a consequence of multiphoton components added to mode i1 (i.e., under the emergence of an imbalance between the thermal mean photon numbers), which leads to coincidence counts at zero delay, hence a reduction in visibility. However, with increasing $\bar{n}_{i2}$, the imbalance between $\bar{n}_{i1,th}$ and $\bar{n}_{i2}$ is reduced, yielding an improvement in the visibility. The interplay between the thermal fields indicates the engagement of multiphoton components of the heralded state in the quantum interference.

Our approach allows for the determination of the nonclassicality degree of a heralded state [35], which depends on the average photon number of its multiphoton components. A negative Mandel parameter ($Q_M < 0$) is sufficient to classify a field as nonclassical [34,36,37]. For a heralded state $Q_M = (\bar{n}_{i1,th}^2 - 1)/(\bar{n}_{i1,th} + 1)$, from which we derive an upper bound on the average photon number of its multiphoton components $\bar{n}_{i1,th} < 1$ to realize nonclassicality. This condition corresponds to a lower bound on the peak visibility of the heralded state's HOM effect with a thermal field, such that for visibilities $V > 41.4\%$ the heralded state can be classified as nonclassical. As depicted in Fig. 5, HOM visibility varies with the average photon number $\bar{n}_{i2}$ of a thermal field. Two cases are presented: HOM between a heralded state and a thermal field (solid curves) and HOM between two thermal fields (dashed curves). The solid curves follow equation (3), whereas the dashed curves are based on the equation in Sec. IX of [24]. In the case of HOM between two thermal fields, the maximum visibility reaches approximately 33.33%.

For two thermal fields in i1 and i2 (see Secs. IX and X [24]), realized by discarding heralding detections on D3, the theoretical $V_{\text{theory}} \approx 33.32\%$ and experimental $V_{\text{exp}} = 28.4\% \pm 3.1\%$ visibilities were obtained that fell below the upper limit of $\sim 33.33\%$ [38] set for the HOM effect between two thermal fields, hence affirming the validity of our approach and analysis. While photon number resolving detectors could enhance heralded state statistical characterization, their limited detection efficiencies and substantial timing jitters hinder their adoption in quantum photonic labs [39]. Our results provide insights into the HOM effect and propose using controlled higher intensities of heralded states for MDI-QKD protocols, which can improve the key rate, speed up the process, and reduce statistical fluctuations in information processing.

This research was funded by the German Research Foundation (EXC 2122, Project ID 390833453); European Research Council (Grant Agreement No. 947603 (QFreC project)); Federal Ministry of Education and Research (PQuMal project, Quantum Futur Program); EPSRC (EP/V062492/1).

[1] H. J. Kimble, The quantum internet, Nature (London) **453**, 1023 (2008).
[2] J. Biamonte, M. Faccin, and M. De Domenico, Complex networks from classical to quantum, Commun. Phys. **2**, 1 (2019).
[3] W. Kozlowski and S. Wehner, Towards large-scale quantum networks, *Proceedings of the 6th ACM International Conference on Nanoscale Computing Communication NANOCOM 2019* (Association for Computing Machinery, NEW York, 2019).
[4] Y. H. Deng, H. Wang, X. Ding, Z. C. Duan, J. Qin, M. C. Chen, Y. He, Y. M. He, J. P. Li, Y. H. Li, L. C. Peng, E. S. Matekole, T. Byrnes, C. Schneider, M. Kamp, D. W. Wang, J. P. Dowling, S. Höfling, C. Y. Lu, M. O. Scully, and J. W. Pan, Quantum interference between light sources separated by 150 million kilometers, Phys. Rev. Lett. **123**, 1 (2019).
[5] C. K. Hong, Z. Y. Ou, and L. Mandel, Measurement of subpicosecond time intervals between two photons by interference, Phys. Rev. Lett. **59**, 2044 (1987).
[6] M. G. Raymer, S. J. van Enk, C. J. McKinstrie, and H. J. McGuinness, Interference of two photons of different color, Opt. Commun. **283**, 747 (2010).
[7] F. Bouchard, A. Sit, Y. Zhang, R. Fickler, F. M. Miatto, Y. Yao, F. Sciarrino, and E. Karimi, Two-photon interference: The Hong-Ou-Mandel effect, Rep. Prog. Phys. **84**, 012402 (2021).
[8] M. Kues, C. Reimer, P. Roztocki, L. R. Cortés, S. Sciara, B. Wetzel, Y. Zhang, A. Cino, S. T. Chu, B. E. Little, D. J. Moss, L. Caspani, J. Azaña, and R. Morandotti, On-chip generation of high-dimensional entangled quantum states and their coherent control, Nature (London) **546**, 622 (2017).
[9] J. M. Lukens and P. Lougovski, Frequency-encoded photonic qubits for scalable quantum information processing, Optica **4**, 8 (2017).
[10] J. D. Siverns, X. Li, and Q. Quraishi, Ion-photon entanglement and quantum frequency conversion with trapped $\hat{Ba}^{+}$ Ions, Appl. Opt. **56**, B222 (2017).
[11] M. Mirhosseini, A. Sipahigil, M. Kalaee, and O. Painter, Superconducting qubit to optical photon transduction, Nature (London) **588**, 599 (2020).
[12] A. Khodadad Kashi and M. Kues, Spectral Hong-Ou-Mandel interference between independently generated single photons for scalable frequency-domain quantum processing, Laser Photonics Rev. **15**, 1 (2021).
[13] Y. L. Tang, H. L. Yin, S. J. Chen, Y. Liu, W. J. Zhang, X. Jiang, L. Zhang, J. Wang, L. X. You, J. Y. Guan, D. X. Yang, Z. Wang, H. Liang, Z. Zhang, N. Zhou, X. Ma, T. Y. Chen, Q. Zhang, and J. W. Pan, Measurement-device-independent quantum key distribution over 200 Km, Phys. Rev. Lett. **113**, 110311 (2014).
[14] A. Rubenok, J. A. Slater, P. Chan, I. Lucio-Martinez, and W. Tittel, Real-world two-photon interference and proof-of-principle quantum key distribution immune to detector attacks, Phys. Rev. Lett. **111**, 130501 (2013).
[15] J. Kołodyński, A. Máttar, P. Skrzypczyk, E. Woodhead, D. Cavalcanti, K. Banaszek, and A. Acín, Device-independent quantum key distribution with single-photon sources, Quantum **4**, 1 (2020).
[16] H. K. Lo, M. Curty, and B. Qi, Measurement-device-independent quantum key distribution, Phys. Rev. Lett. **108**, 130503 (2012).
[17] A. Christ and C. Silberhorn, Limits on the deterministic creation of pure single-photon states using parametric down-conversion, Phys. Rev. A **85**, 023829 (2012).
[18] S. K. Liao *et al.*, Satellite-to-ground quantum key distribution, Nature (London) **549**, 43 (2017).
[19] A. Mizutani, K. Tamaki, R. Ikuta, T. Yamamoto, and N. Imoto, Measurement-device-independent quantum key distribution for scarani-acin-ribordy-gisin 04 protocol, Sci. Rep. **4**, 5236 (2014).
[20] C. Wang, F.-X. Wang, H. Chen, S. Wang, W. Chen, Z.-Q. Yin, D.-Y. He, G.-C. Guo, and Z.-F. Han, Realistic device imperfections affect the performance of Hong-Ou-Mandel interference with weak coherent states, J. Lightwave Technol. **35**, 4996 (2017).
[21] Q. Wang, X.-Y. Zhou, and G.-C. Guo, Realizing the measure-device-independent quantum-key-distribution with passive heralded-single photon sources, Sci. Rep. **6**, 35394 (2016).
[22] X. Li, L. Yang, L. Cui, Z. Y. Ou, and D. Yu, Observation of quantum interference between a single-photon state and a thermal state generated in optical fibers, Opt. Express **16**, 12505 (2008).
[23] H.-L. Yin, Y. Fu, Y. Mao, and Z.-B. Chen, Security of quantum key distribution with multiphoton components, Sci. Rep. **6**, 29482 (2016).
[24] See Supplemental Material at http://link.aps.org/supplemental/10.1103/PhysRevLett.131.233601 for detailed calculations.
[25] D. B. Horoshko, S. De Bièvre, G. Patera, and M. I. Kolobov, Thermal-difference states of light: Quantum states of heralded photons, Phys. Rev. A **100**, 053831 (2019).
[26] R. Wiegner, J. Von Zanthier, and G. S. Agarwal, Quantum interference and non-locality of independent photons from

disparate sources, J. Phys. B At. Mol. Opt. Phys. **44**, 055501 (2011).
[27] Rodney Loudon, *The Quantum Theory of Light* (Oxford University Press, Oxford, 2010).
[28] B. Bai, Y. Zhou, R. Liu, H. Zheng, Y. Wang, F. Li, and Z. Xu, Hanbury Brown–Twiss effect without two-photon interference in photon counting regime, Sci. Rep. **7**, 1 (2017).
[29] A. Khodadad Kashi, L. Sader, R. Haldar, B. Wetzel, and M. Kues, Frequency-to-time mapping technique for direct spectral characterization of biphoton states from pulsed spontaneous parametric processes, Front. Photonics **3**, 834065 (2022).
[30] M. Giovannini, Hanbury Brown–Twiss interferometry and second-order correlations of inflaton quanta, Phys. Rev. D **83**, 023515 (2011).
[31] H. H. Lu, J. M. Lukens, N. A. Peters, O. D. Odele, D. E. Leaird, A. M. Weiner, and P. Lougovski, Electro-optic frequency beam splitters and tritters for high-fidelity photonic quantum information processing, Phys. Rev. Lett. **120**, 030502 (2018).
[32] J. Liu, Y. Zhou, W. Wang, R. Liu, K. He, F. Li, and Z. Xu, Spatial second-order interference of pseudothermal light in a Hong-Ou-Mandel interferometer, Opt. Express **21**, 19209 (2013).
[33] Z.-Y. J. Ou, *Multi-Photon Quantum Interference* (Springer US, Boston, MA, 2007), Vol. 53.
[34] S. Signorini and L. Pavesi, On-chip heralded single photon sources, AVS Quantum Sci. **2**, 041701 (2020).
[35] P. M. Alsing, R. J. Birrittella, C. C. Gerry, J. Mimih, and P. L. Knight, Extending the Hong-Ou-Mandel effect: The power of nonclassicality, Phys. Rev. A **105**, 013712 (2022).
[36] G. S. Agarwal, *Quantum Optics* (Cambridge University Press, Cambridge, England, 2012).
[37] S. M. Barnett, G. Ferenczi, C. R. Gilson, and F. C. Speirits, Statistics of photon-subtracted and photon-added states, Phys. Rev. A **98**, 013809 (2018).
[38] Z. Y. Ou, J. K. Rhee, and L. J. Wang, Photon bunching and multiphoton interference in parametric down-conversion, Phys. Rev. A **60**, 593 (1999).
[39] R. H. Hadfield, Single-photon detectors for optical quantum information applications, Nat. Photonics **3**, 696 (2009).